A generalized method of converting CT image to PET linear attenuation coefficient distribution in PET/CT imaging*

Wang Lu(王 璐)[a)b)], Wu Li-Wei(武丽伟)[a)b)], Wei Le(魏 乐)[a)b)], Gao Juan(高 娟)[a)c)], Sun Cui-Li(孙翠丽)[a)c)], Chai Pei(柴 培)[a)c)†], and Li Dao-Wu(李道武)[a)c)]

[a)] *Key Laboratory of Nuclear Radiation and Nuclear Energy Technology, Institute of High Energy Physics, Chinese Academy of Sciences, Beijing* 100049, *China*

[b)] *University of Chinese Academy of Sciences, Beijing* 100049, *China*

[c)] *Beijing Engineering Research Center of Radiographic Techniques and Equipment, Beijing* 100049, *China*

(Received 19 April 2013; revised manuscript received 24 May 2013; published online 10 December 2013)

The accuracy of attenuation correction in positron emission tomography scanners depends mainly on deriving the reliable 511-keV linear attenuation coefficient distribution in the scanned objects. In the PET/CT system, the linear attenuation distribution is usually obtained from the intensities of the CT image. However, the intensities of the CT image relate to the attenuation of photons in an energy range of 40 keV–140 keV. Before implementing PET attenuation correction, the intensities of CT images must be transformed into the PET 511-keV linear attenuation coefficients. However, the CT scan parameters can affect the effective energy of CT X-ray photons and thus affect the intensities of the CT image. Therefore, for PET/CT attenuation correction, it is crucial to determine the conversion curve with a given set of CT scan parameters and convert the CT image into a PET linear attenuation coefficient distribution. A generalized method is proposed for converting a CT image into a PET linear attenuation coefficient distribution. Instead of some parameter-dependent phantom calibration experiments, the conversion curve is calculated directly by employing the consistency conditions to yield the most consistent attenuation map with the measured PET data. The method is evaluated with phantom experiments and small animal experiments. In phantom studies, the estimated conversion curve fits the true attenuation coefficients accurately, and accurate PET attenuation maps are obtained by the estimated conversion curves and provide nearly the same correction results as the true attenuation map. In small animal studies, a more complicated attenuation distribution of the mouse is obtained successfully to remove the attenuation artifact and improve the PET image contrast efficiently.

Keywords: linear attenuation coefficient, PET/CT, attenuation correction, consistency conditions

PACS: 78.70.–g, 87.57.uk, 87.59.Q–, 87.57.C– **DOI:** 10.1088/1674-1056/23/2/027802

1. Introduction

Accurate attenuation correction is required in positron emission tomography (PET) imaging for image artifact removal and quantitative studies.[1,2] The accuracy of correction depends mainly on deriving the reliable PET 511-keV linear attenuation coefficient distribution from the scanned objects.[3,4]

A current trend is to combine PET and computed tomography (CT) into a union imaging system PET/CT. In this system, the linear attenuation distribution is usually obtained from the CT scan. CT images provide lower-noise and higher-resolution tissue density information in a very short time, but the intensities of CT images relate to the attenuation of photons in an energy range of 40 keV–140 keV. Before implementing PET attenuation correction, the intensities of the CT image must be transformed into the PET 511-keV linear attenuation coefficients.[5–7]

Several methods have been developed to convert CT image into PET linear attenuation distribution.[6,8,9] These methods are shown to yield good results in a number of situations; however, they often encounter their problems because the CT scan parameters can affect the effective energy of CT X-ray photons and thus affect the intensities of the CT image. Before implementing PET attenuation correction, the CT voxel values in terms of intensity should be converted into the 511-keV linear attenuation coefficients using the corresponding conversion curve. For each set of CT scan parameters such as a pair of tube voltage and tube current, a corresponding conversion curve needs to be calculated separately.[2,8,9] Therefore, the phantom calibration experiment must be implemented to determine the conversion curve for a given set of CT scan parameters. This manner lacks convenience and robustness, especially when some sudden scan parameters are required.

In this work, we develop a generalized method based on consistency conditions for transforming CT images for PET attenuation correction without any calibration experiments. The reliability of the proposed method is evaluated with phantom experiments and small animal experiments using a small animal PET/CT scanner developed by the Institute of High Energy Physics, Chinese Academy of Sciences.

*Project supported by the National Natural Science Foundation of China (Grant Nos. 81101070 and 81101175).

†Corresponding author. E-mail: chaipei@ihep.ac.cn

© 2014 Chinese Physical Society and IOP Publishing Ltd

2. Theory

2.1. Consistency conditions

The Helgason–Ludwig consistency conditions are a set of mathematical rules. They are derived from the Radon transform and are satisfied by perfect PET data, such as attenuation corrected data. Natterer's formulation of the consistency conditions for PET data is given by[10,11]

$$\int_0^{2\pi}\int_{-\infty}^{+\infty} s^m \mathrm{e}^{\mathrm{i}k\phi}\,\mathrm{e}^{T(s,\phi)}E(s,\phi)\,\mathrm{d}s\,\mathrm{d}\phi = 0. \quad (1)$$

Here, $E(s,\phi)$ is the emission sinogram acquired by PET; $T(s,\phi)$ is the transmission sinogram which can be obtained from the radon transform of the PET attenuation map; m determines the moment, which is an integer greater than or equal to zero and k determines the Fourier component, which is an integer and satisfies that k is greater than m or $k+m$ is odd; s is the radial distance from the center of rotation in the radon transform space; ϕ is the azimuthal angle of rotation in the radon transform space.

With the given emission sinogram, the attenuation map can be calculated by solving the above equations of consistency conditions. Solving these equations is equivalent to minimizing the following objective function:[12,13]

$$F_{m,k} = \sum_{0\le m<k}\left\|\int_0^{2\pi}\int_{-\infty}^{+\infty} s^m \mathrm{e}^{\mathrm{i}k\phi}\,\mathrm{e}^{T(s,\phi)}E(s,\phi)\,\mathrm{d}s\,\mathrm{d}\phi\right\|^2. \quad (2)$$

2.2. Conversion model

In practice, the objective function may have many local minima due to the poor signal-to-noise ratio in PET data. Therefore, it is necessary to regularize the problem and narrow the search space by using some prior information about the attenuation map.[14–17] For the work presented here, it is assumed that the attenuation map can be obtained from the CT image through the following quadratic polynomial conversion:[2,9]

$$\mu_{\mathrm{PET}} = AI_{\mathrm{CT}}^2 + BI_{\mathrm{CT}} + C. \quad (3)$$

In Eq. (3), I_{CT} is the voxel value of a given voxel in the registered CT image, which is represented in terms of intensity; μ_{PET} is the attenuation coefficient of the corresponding voxel in the attenuation map; A, B, and C are the conversion factors.

After PET/CT image registration, we convert the registered CT image into the initial attenuation map using Eq. (3) with the initial conversion factors. The initial attenuation map provides the prior information for the consistency conditions.

2.3. Implementation of optimization

The Levenberg–Marquardt algorithm (LM algorithm) is used to estimate the conversion factors and minimize the objective function. During each iteration procedure, the CT image is converted into the attenuation map using Eq. (3) with the current estimates of conversion factors, and then the linear integration of the updated attenuation map is calculated to provide the transmission sinogram in Eq. (2). The objective function is evaluated by calculating Eq. (2) with some certain values of m and k. In this study, we use the data set $\{m = 1,2; k \in N\}$, which satisfies the conditions that $m < k < 9$ and $k+m$ is odd. The stopping rule of the algorithm is that there is less than 0.1% change in the objective function with the following penalties: (i) each attenuation coefficient in the attenuation map is above or equal to zero; (ii) after the conversion, each voxel whose intensity is zero in the CT image remains zero in the attenuation map, which implies that the constant term "C" in Eq. (3) should be zero; (iii) the conversion curve is convex to the below.[2] Before the optimization, the initial conversion factors are randomly generated. There are fewer restrictions on the random variables but the converting of the registered CT image into the initial attenuation map with the variables should follow Rules (i)–(iii) mentioned above.

2.4. Procedure and comparison

Figure 1 shows the procedures of the original method based on the phantom calibration experiments, and the proposed method based on consistency conditions.

For the first, the CT phantom experiments must be implemented to determine different conversion factors with various sets of usual CT scan parameters. The phantom is specially designed for the calibration experiments, and it contains various materials which have typical linear attenuation coefficients. To acquire the conversion curve, the 511-keV linear attenuation coefficients of materials are first calculated using the NIST data tables.[18] Then, the regions of interest (ROIs) representing the materials are outlined in CT images, and the mean values of voxels in the ROIs are calculated. Therefore, some scatter points are acquired which represent the voxel values of materials in CT images and the 511-keV linear attenuation coefficients of materials. Finally, the conversion curve and conversion factors are calculated in quadratic polynomial fitting of the scatter points. When a set of CT scan parameters has been chosen for a PET/CT scan, if the conversion factors have been acquired in the previous phantom calibration experiments under the same CT scan parameter conditions, the attenuation map can be obtained by converting the CT image using these factors. However, if the CT scan parameters are not included in the previous phantom calibration experiments, an extra phantom experiment is necessary to obtain the conversion factors with current parameters.

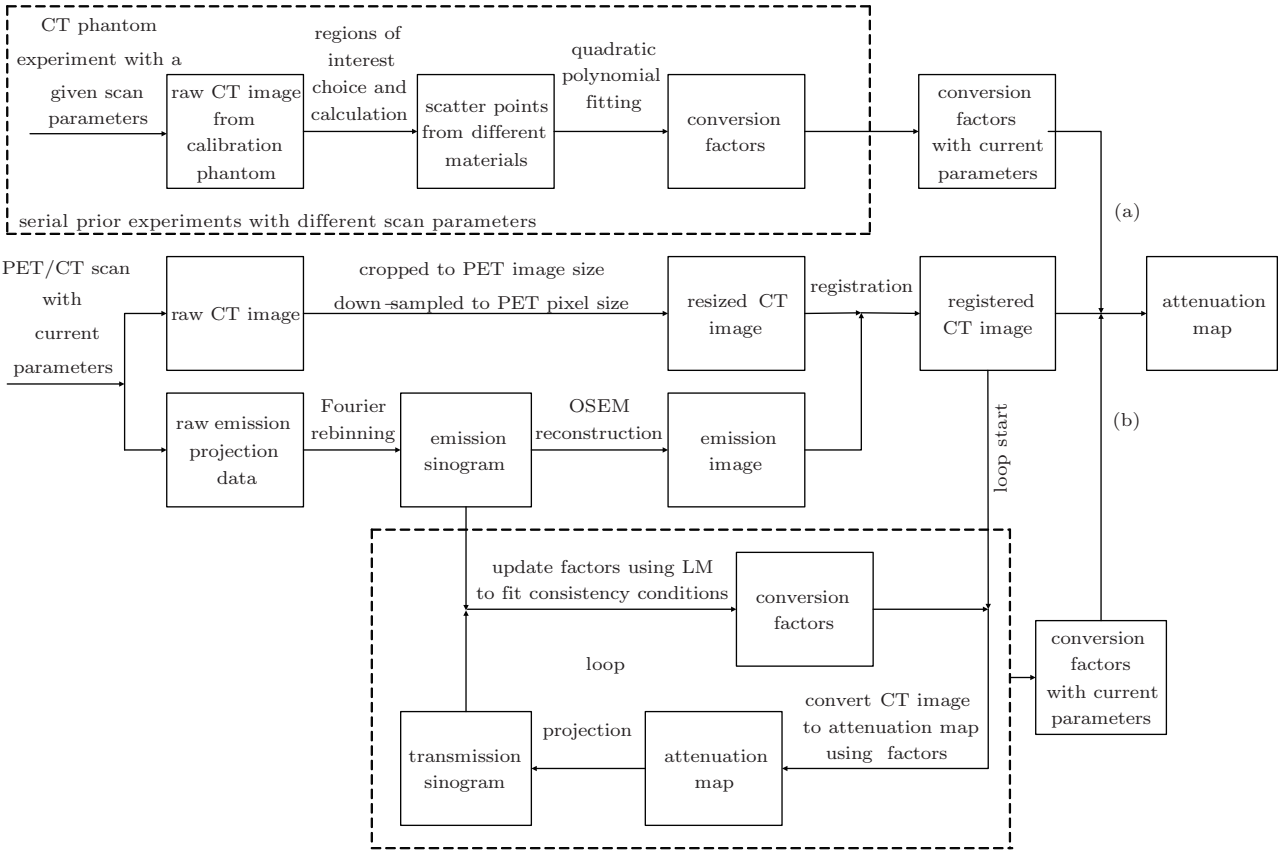


Fig. 1. Procedures of (a) the original method based on the phantom calibration experiments and (b) the proposed method based on consistency conditions.

On the other hand, for any set of CT scan parameters, the proposed method can achieve the transformation of CT image into attenuation map but not depend on the phantom calibration experiment. The conversion factors can be calculated directly by employing the consistency conditions to yield the most consistent attenuation map with the measured PET data as mentioned in Subsection 2.1 to 2.3.

3. Methods and results

3.1. Data acquisition and processing

Data were acquired for all studies in this work using a small animal PET/CT scanner, which was developed by the Institute of High Energy Physics, Chinese Academy of Sciences.

In the PET subsystem of this scanner LYSO-based detector blocks, having an 11-cm transaxial field-of-view (FOV), a 6.4-cm axial FOV, a central point source with a spatial resolution of 1.85-mm full-width at half-maximum (FWHM) and sensitivity of 2.38% at the center, were used. PET scans were acquired with a 360 keV–660 keV energy window and 6-ns timing window. The emission projection data were acquired in listmode format and Fourier-rebinned[19] into two-dimensional (2D) sinograms. Images were then reconstructed using the 2D OSEM algorithm[20] (four iterations and sixteen subsets), resulting in 0.5 mm×0.5 mm×1.0 mm voxel size for a 256×256×63 image volume. Except attenuation, the PET images were corrected for detector efficiency, dead-time, radioactive decay, and photon scatter.

The CT subsystem includes a standard self-contained, air-cooled X-ray tube operating at a maximum tube voltage of 90 kV and a maximum tube current of 200 μA. CT scans were acquired by using CT tube voltages varying between 0 and 90 kVp and by optimizing the tube current. The gantry rotated in continuous flying mode. A total of 360 projections were acquired in a full 360° scan with a 1024×360 projection matrix size. The CT images were reconstructed using a 3D cone-beam Feldkamp algorithm into 0.25 mm×0.25 mm×0.25mm voxel size in a 512×512×512 image matrix. After being cropped to PET image size, down-sampled to PET voxel size, the registered CT images were then acquired with an affine transform and linear interpolation.

3.2. Phantom studies

In this study, we designed a cylindrical phantom ($\phi = 40 \pm 0.5$ mm) within four small hollow cylinders ($\phi = 8 \pm 0.5$ mm). This phantom can also be used for the original method based on the phantom calibration experiments.[2] For comparison, we scanned the phantom with three different sets of CT scan parameters and determined the three sets of con-

version curves using the proposed method and the original calibration method.

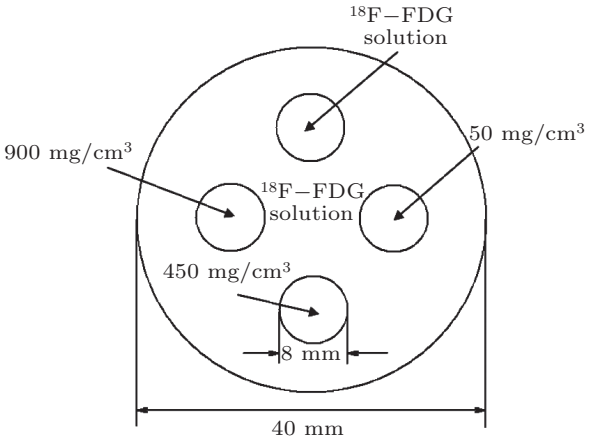


Fig. 2. Hollow cylindrical phantom with four small hollow cylinders.

The phantom and the cylinders were all made of plexiglass, each of which had a similar attenuation coefficient to that of water. As shown in Fig. 2, the phantom was filled with a uniformly distributed mixture of water and 1.17-mCi of ^{18}F–FDG. One of the four small cylinders was filled with the same mixture above, which represented water and had the same attenuation coefficient as that of water, and the other three were filled with a mixed solution of water and K_2HPO_4 with concentrations of 50 mg/cm^3, 450 mg/cm^3, and 900 mg/cm^3.

The emission data of the phantom were acquired from a 10-minute PET scan, and then three sets of transmission data of the phantom were acquired from three corresponding CT scans by varying CT tube voltages from 60 kVp to 80 kVp but keeping the tube current unchanged (here it was 40 μA). As mentioned in Subsection 3.1, both the raw CT images and the PET images were reconstructed. After the raw CT images were cropped to PET image size and down-sampled to PET voxel size, the registered CT images were acquired by aligning the center of each cylinder from the PET and registered CT images.

Table 1 shows the scatter points in the CT images with various CT tube voltages. The scatter points represent the corresponding solutions in the four cylinders and are acquired as mentioned in Subsection 2.4. The fitting conversion curve of the scatter points from Table 1 and the estimated conversion curve using the proposed method are shown in Fig. 3. Note that Hounsfield units could be a middle step for transforming the raw CT data to the PET 511-keV attenuation coefficients; however, it is not a necessary step and is skipped in this paper.[2]

Table 1. Scatter points in the CT images with various CT tube voltages which represent the corresponding solutions in the four cylinders.

Materials		I_{CT}/unit			μ_{PET}/cm^{-1}
		60 kVp	70 kVp	80 kVp	
Water		3754.1±392.3	4065.9±351.4	4226.2±321.0	0.096
K_2HPO_4/(mg/cm^3)	50	4152.0±407.3	4451.9±365.4	4603.1±336.7	0.101
	450	6573.5±868.3	6832.1±756.1	6886.7±683.8	0.136
	900	8481.1±936.2	8728.6±657.1	8677.3±597.8	0.175

As shown in Fig. 3, the estimated conversion curve can fit the scatter points accurately and can provide a proper transformation for each given CT tube voltage. Though the differences can also be observed between the proposed method and the original method, they are located in a range of standard deviation variances from the voxel values of the scatter points.

To quantitatively evaluate the accuracy of transformation above and the effect of the difference between these two methods, we calculated the mean values of linear attenuation coefficients of four cylinders in the attenuation maps from the proposed method and the original calibration method, and then we listed the deviations between these mean values (μ_{mean}) and the true linear attenuation coefficients (μ_{true}), as shown in Table 2. Here the true linear attenuation coefficients are calculated using the NIST data tables as mentioned in Subsection 2.4. Due to the lower dose of ^{18}F–FDG in the solution, the calculated coefficient of the ^{18}F–FDG solution is the same as that of water. We have the following deviation definition:

$$\text{bias} = \frac{\mu_{mean} - \mu_{true}}{\mu_{true}} \times 100\%. \quad (4)$$

The results show that after the transformations of CT images into attenuation maps, the attenuation coefficients obtained by both of these methods accord with the true coefficients. Furthermore, the results also show that at 70 kVp and 80 kVp, some slight differences still exist between the estimated coefficients and the fitting coefficients. Here the estimated coefficients are from the attenuation maps acquired by the proposed method, and the fitting coefficients are from the attenuation maps acquired by the fitting conversion curves. Comparing the linear attenuation coefficients at these two tube voltages with the true ones, the estimated coefficients of 900 mg/cm^3 K_2HPO_4 solutions are closer to the true ones but the fitting coefficients of 450 mg/cm^3 K_2HPO_4 solutions

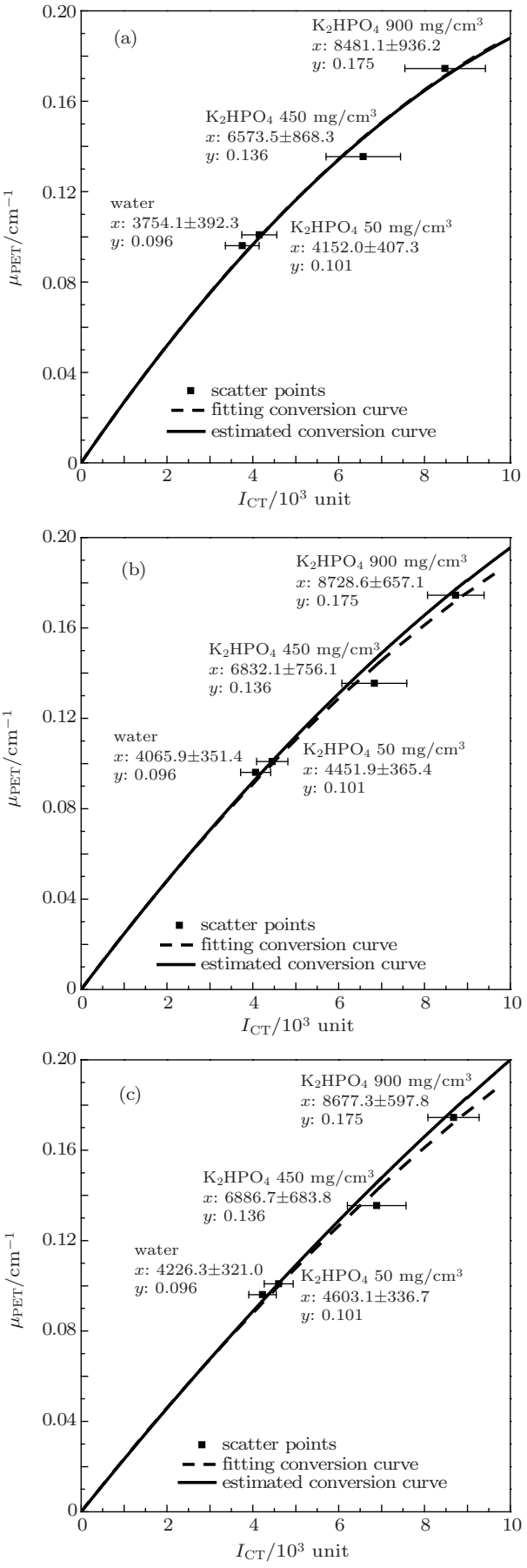


Fig. 3. Fitting conversion curves of scatter points from Table 1 and the estimated conversion curves using the proposed method with various CT tube voltages: (a) 60 kVp; (b) 70 kVp; (c) 80 kVp.

are closer to the true ones, and for the water and 50 mg/cm^3 K_2HPO_4 solutions, the two methods provide nearly the same coefficients.

Table 2. Mean values of linear attenuation coefficients of four cylinders in the obtained attenuation maps with various CT tube voltages: (a) 60 kVp, (b) 70 kVp, and (c) 80 kVp, and the deviations between them and the true 511-keV linear attenuation coefficients.

(a) 60 kVp

μ_{PET}/cm^{-1}	Water	K_2HPO_4/(mg/cm^3)		
		50	450	900
True	0.096	0.101	0.136	0.175
Estimated	0.092±0.002	0.099±0.003	0.144±0.009	0.171±0.009
(Bias)	(–4.2%)	(–2.0%)	(+5.9%)	(–2.3%)
Fitting	0.092±0.002	0.099±0.003	0.144±0.009	0.171±0.009
(Bias)	(–4.2%)	(–2.0%)	(+5.9%)	(–2.3%)

(b) 70 kVp

μ_{PET}/cm^{-1}	Water	K_2HPO_4/(mg/cm^3)		
		50	450	900
True	0.096	0.101	0.136	0.175
Estimated	0.093±0.002	0.100±0.003	0.146±0.010	0.176±0.007
(Bias)	(–3.1%)	(–1.0%)	(+7.4%)	(+0.6%)
Fitting	0.092±0.002	0.099±0.003	0.143±0.010	0.169±0.013
(Bias)	(–4.2%)	(–2.0%)	(+5.1%)	(–3.4%)

(c) 80 kVp

μ_{PET}/cm^{-1}	Water	K_2HPO_4/(mg/cm^3)		
		50	450	900
True	0.096	0.101	0.136	0.175
Estimated	0.093±0.002	0.100±0.003	0.145±0.010	0.177±0.008
(Bias)	(–3.1%)	(–1.0%)	(+6.6%)	(+1.1%)
Fitting	0.093±0.002	0.100±0.003	0.142±0.010	0.170±0.012
(Bias)	(–3.1%)	(–1.0%)	(+4.4%)	(–2.9%)

In order to evaluate the influences of differences between the estimated coefficients and the true ones on attenuation correction, the attenuation correction factors were calculated from the estimated attenuation maps and were used to correct the PET attenuation artifacts. The PET images were reconstructed in the following ways: i) using the true attenuation maps of phantom and ii) using the estimated maps from the proposed method.

Figure 4 shows the reconstructed PET images from a typical transaxial slice of phantom before and after the correction, and the profiles are also shown.

As shown in Fig. 4, though the attenuation maps are converted from different CT images with three tube voltages, the corrected PET images are nearly the same. Although the phantom is scanned with different CT tube voltages, it has the unique linear attenuation coefficient distribution at 511 keV. As a result, the proposed method provides a proper conversion curve for each CT image with a given CT tube voltage and converts each CT image into the unique attenuation map for PET attenuation correction. Moreover, the results also indicate that the deviations between the estimated coefficients and the true coefficients have few influences on the accuracy of attenuation correction, which can work as well as the correction using the true attenuation maps.

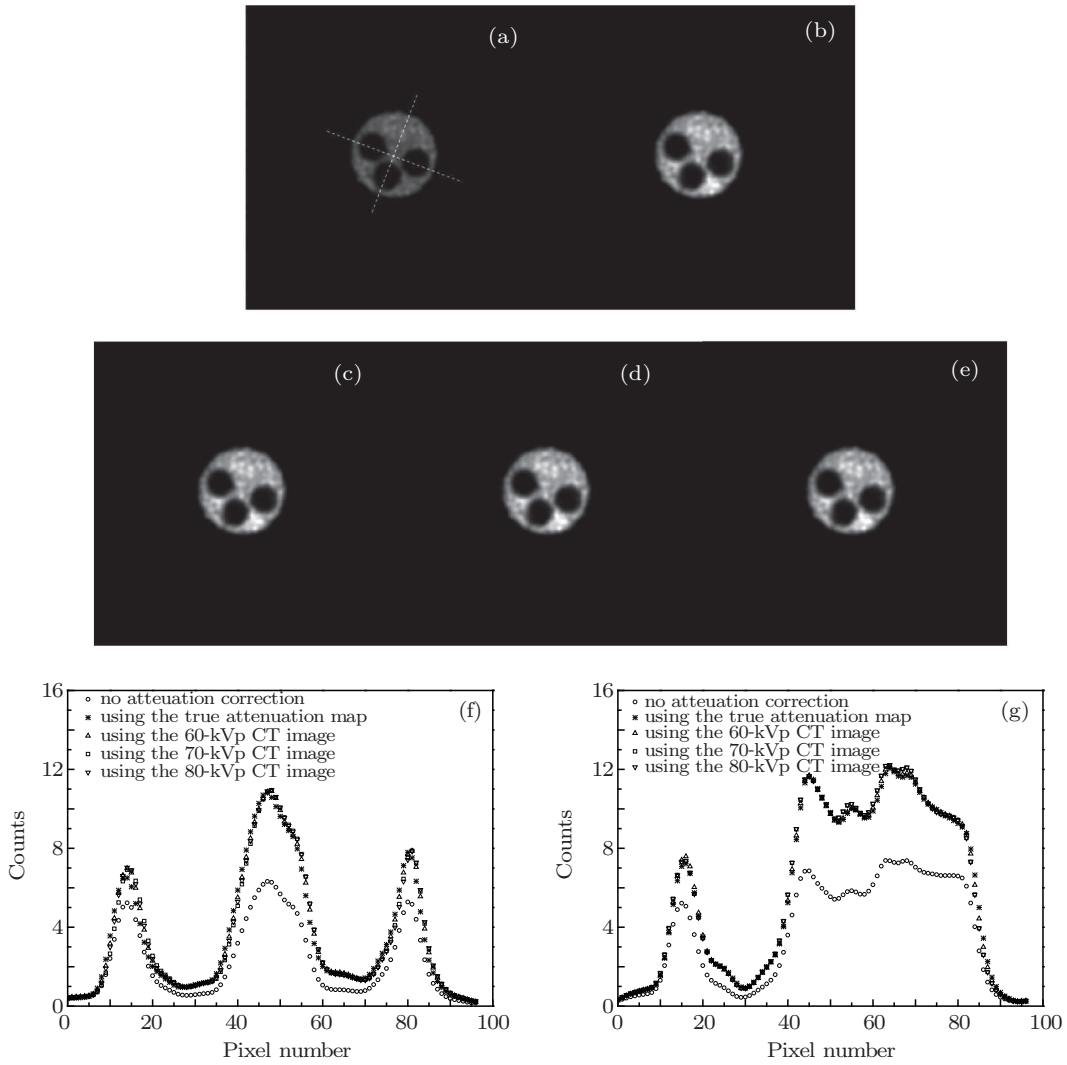


Fig. 4. The reconstructed PET images from the typical slice of phantom performed by (a) no attenuation correction; (b) the attenuation correction using the true attenuation map; the attenuation correction using the proposed method, and the CT images at the tube voltages of (c) 60 kVp, (d) 70 kVp, and (e) 80 kVp. Panels (f) and (g) show the profiles through the images of no attenuation correction and the attenuation correction.

3.3. Small animal studies

To evaluate the validity of the proposed method for some more complicated attenuation maps, a mouse was injected with the solution of water and 1.17 mCi of ^{18}F–FDG for small animal studies. After about a 30-minute uptake period, the mouse was sacrificed and fixed with tape to the imaging bed of the scanner. Then the CT imaging was implemented with the tube voltage at 45 kVp and the tube current at 15 μA. Following the CT scan, the PET imaging was implemented. Finally, as mentioned in Subsection 3.1, both the raw CT images and the PET images were reconstructed, and the registered CT images were acquired.

In fact, the effective attenuation coefficient depends on the amount of scatter, which may vary with the size and structure of the scanned objects. For the same scan parameters, the conversion curve from the phantom calibration experiment may be not accurate enough for the small animal, unless the phantom has the same size and structure as that of the small animal. Therefore, few direct evidences can be used to quantify the accuracy of attenuation correction in small animal studies, even after some phantom experiments have been implemented.[2]

To acquire more accurate scatter points for the curve fitting and compare the fitting conversion curve with the estimated curve obtained by the proposed method, we segment the registered CT images and outline the ROIs of three typical mouse tissues, i.e., bone, soft tissue, and lung. Then the mean values of voxels in the ROIs are calculated. The scatter points from the attenuation coefficients of three typical tissues[3] and their corresponding CT voxel values are indicated in Fig. 5, and figure 5 also shows the estimated conversion curves and the fitting conversion curves for the mouse.

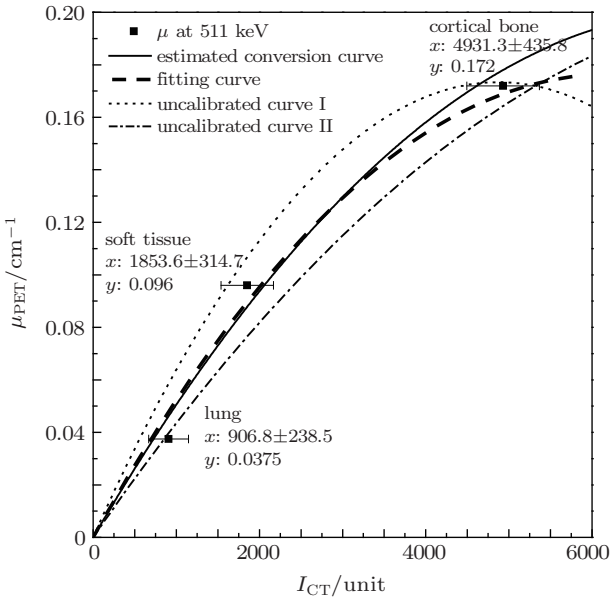


Fig. 5. Estimated conversion curves using the proposed method and the fitting conversion curves for the mouse, and the two uncalibrated curves for comparison used in the following section.

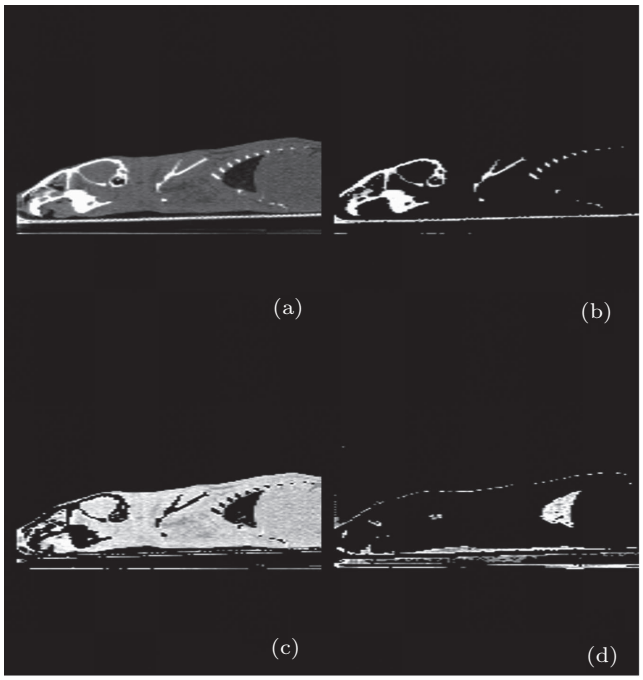


Fig. 6. (a) Estimated attenuation map from the mouse and the sub-images of (b) the bone segmentation, (c) the soft tissue segmentation, and (d) the lung segmentation. Each image above is shown in its full range contrast.

In Fig. 6, the attenuation map is obtained using the estimated curve in Fig. 5. To quantitatively evaluate the accuracy of conversion, some images (shown in Fig. 6) are segmented from the attenuation map using the corresponding thresholds, and the mean values of attenuation coefficients for each tissue in the segmented images are calculated in Table 3. The segmented thresholds are empirically chosen by referring to the attenuation coefficients of tissues, as follows: (i) above 0.12 cm^{-1} for bone; (ii) from 0.06 cm^{-1} to 0.12 cm^{-1} for soft tissue; (iii) from 0.025 cm^{-1} to 0.06 cm^{-1} for lung inhale and lung exhale.

For comparisons, two uncalibrated curves (the uncalibrated curve I and the uncalibrated curve II in Fig. 5) are also obtained. The two sets of uncalibrated scatter points are created using the mean values of voxels of the calibrated scatter points in Fig. 5 minus or plus their standard deviations. Therefore, the other three attenuation maps are obtained using the fitting curve and the two uncalibrated curves. Similarly, the three attenuation maps are segmented and the mean values of attenuation coefficients for each tissue in these segmented images are also calculated in Table 3.

Table 3. Mean values of linear attenuation coefficients for each tissue in the sub-images comparing with the true attenuation coefficients.

	μ_{PET}/cm^{-1}		
	Lung	Soft tissue	Bone
True	0.0375	0.096	0.172 (cortical)
Estimated	0.042±0.010	0.093±0.010	0.163±0.026
(Bias)	(+12.0%)	(–3.1%)	(–5.2%)
Fitting	0.042±0.010	0.094±0.010	0.152±0.018
(Bias)	(+12.0%)	(–2.1%)	(–11.6%)
Uncalibrated I	0.041±0.011	0.105±0.014	0.143±0.019
(Bias)	(+9.3%)	(+9.4%)	(–16.9%)
Uncalibrated II	0.040±0.010	0.083±0.010	0.162±0.027
(Bias)	(+6.7%)	(–13.5%)	(–5.8%)

The results in Fig. 6 show that the proposed method should be robust for the mouse, which has a more complicated attenuation distribution than the phantom shown in Fig. 1. However, as shown in Fig. 6, it is observed that due to the partial volume effect, the lung segmentation map typically includes the voxels from the boundary of soft tissue or CT scan bed, and thus there are likely to be some errors in assigning a lung attenuation coefficient for these voxels. Similarly, the voxels from the CT scan bed can also be observed in the soft tissue segmentation and the bone segmentation. Accordingly, as shown in Table 3, the lung attenuation coefficients from the four curves in Fig. 5 have similar values but larger deviations exist between them and the true coefficient. The results in Table 3 also show that for soft tissue, the estimated curve and the fitting curve provide better estimation than the two uncalibrated curves. For bones, however, the estimation from the fitting curve is a little worse than the estimated curve.

The corrected PET images using the proposed method for the mouse are reconstructed in Fig. 7. The results show that after attenuation correction, the image contrast can be improved effectively, and the attenuation artifacts can be reduced. Therefore, accurate attenuation correction is essential for small animal studies. Meanwhile, as shown in Fig. 7, the attenuation maps from the fitting curve and the two uncalibrated curves are used to obtain the corrected PET images and provide more evaluations among the five conversion curves.

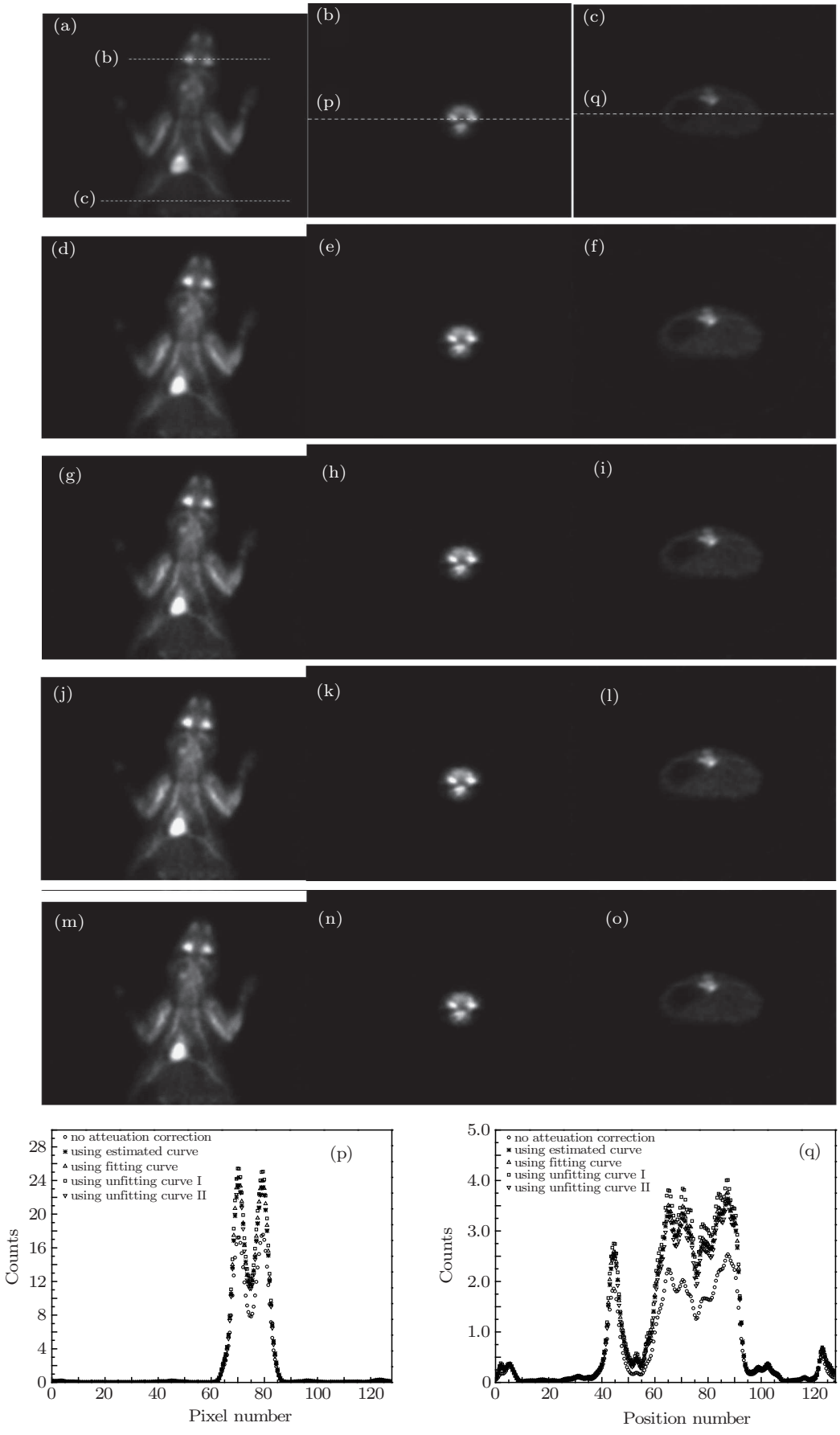


Fig. 7. The PET images from the mouse performed by ((a), (b), and (c)) without attenuation correction; ((d), (e), and (f)) with the attenuation correction using the proposed method; ((g), (h), and (i)) with the attenuation correction using the fitting curve; ((j), (k), and (l)) with the attenuation correction using the uncalibrated curve I; ((m), (n), and (o)) with the attenuation correction using the uncalibrated curve II; ((p) and (q)) corresponding to horizontal profiles passing near the centers of the PET images.

As shown in Figs. 7(d)–7(o), the influences from the differences between attenuation coefficients listed in Table 3 cannot be observed qualitatively. However, the horizontal profiles passing near the centers of the PET images from the two uncalibrated curves can prove the fact that there exist some influences of over-correction or under-correction as shown in Figs. 7(p) and 7(q), and these influences will adversely affect the quantitative studies. Moreover, due to smaller scanned objects and less photon attenuation, there are less influences of over-correction or under-correction in Fig. 7(p) than in Fig. 7(p).

4. Discussion and conclusion

In the phantom studies, the results of phantom experiments show that the proposed method has less dependence on the CT scan parameters and can provide the accurate conversion curve without any calibration experiment. Nevertheless, it is observed in Table 1 that with the decline of tube voltages, the mean values of voxels from the four solutions in the CT images decrease but the standard deviations increase. Though the results in Table 2 indicate that higher standard deviations have few influences on the accuracies of the estimated attenuation coefficients, a more comprehensive analysis is required to determine whether the method can be applied to a broader range of scan parameters. Meanwhile, the results in Fig. 4 also show that the deviations between the estimated attenuation coefficients and the true ones can be ignored in the reconstructed images. However, supposing some sudden situations that the PET images might suffer relatively low activities or the phantom might be enlarged so that worse photon attenuation would happen, the deviations would bring more challenges, which should be considered in further studies.

In the small animal studies, although the true attenuation map of the mouse cannot be obtained to quantify the accuracy of attenuation correction more directly, it is noteworthy that some indirect evidences are given to support the proposed method and verify that the method is capable of dealing with more complicated attenuation distribution. The results in Fig. 5 show that the conversion curve obtained by the proposed method is accurate enough to fit the scatter points from the attenuation coefficients of some tissues and their corresponding CT voxel values. Furthermore, the results in Fig. 6 and Table 3 show that the estimated linear attenuation distribution agrees with the true distribution in visualization and quantification.

It is concluded that the method based on consistency conditions can accurately estimate the conversion curve with a given pair of CT scan parameters and successfully improve the PET image contrast. In future work, we will focus on evaluating the proposed method using broader sets of scan parameters. Furthermore, we will investigate the robustness that the method can be extended to larger and more complicated objects for whole-body PET/CT studies.

References

[1] Konik A, Koesters T, Madsen M T and Sunderland J J 2011 *IEEE Trans. Nucl. Sci.* **58** 2308

[2] Yao R, Seidel J, Liow J and Green M V 2005 *IEEE Trans. Nucl. Sci.* **52** 664

[3] Burger C, Goerres G, Schoenes S, Buck A, Lonn A H and Von Schulthess G K 2002 *Eur. J. Nucl. Med.* **29** 922

[4] Bai C, Shao L, Silva A J D and Zhao Z 2003 *IEEE Trans. Nucl. Sci.* **50** 1510

[5] Kinahan P E, Hasegawa B H and Beyer T 2003 *Semin Nucl. Med.* **33** 166

[6] Yu J, Seidel J, Pomper M and Tsui B M W 2007 *Proc. IEEE Nuclear Science Symposium and Medical Imaging Conference*, October 26–November 3, 2007, Honolulu, HI, USA, p. 3747

[7] Prasad R, Ay M R, Ratib O and Zaidi H 2011 *IEEE Trans. Nucl. Sci.* **58** 66

[8] Zaidi H and Hasegawa B 2003 *J. Nucl. Med.* **44** 291

[9] Shirmohammad M, Ay M R, Sarkar S, Ghadiri H and Rahmim A 2008 *Proc. IEEE International Symposium on Biomedical Imaging: From Nano to Macro*, May 14–17, 2008, Paris, France, p. 644

[10] Natterer F 1986 *the Mathematics of Computerized Tomography* (New York: Wiley) p. 49

[11] Alessio A M, Kinahan P E and Champley K M 2010 *Med. Phys.* **37** 1191

[12] Bromiley A, Welch A, Chilcott F, Waikar S, McCallum S, Dodd M, Craib S, Schweiger L and Sharp P 2002 *IEEE Trans. Nucl. Sci.* **48** 1371

[13] Wang L, Chai P, Wu L W, Yun M K, Zhou X L, Liu S Q, Zhang Y B, Shan B C and Wei L 2013 *Chin. Phys. C* **37** 018201

[14] Gao F, Yamada R, Watanabe M and Liu H F 2009 *Chin. Phys. B* **18** 3066

[15] Yamada R, Watanabe M, Gao F and Liu H F 2009 *Acta Phys. Sin.* **58** 3584 (in Chinese)

[16] Welch A, Campbell C, Clackdoyle R, Natterer F, Mikecz P, Chillcot F, Dodd M, Hopwood P, Craib S, Gullberg G T and Sharp P 1997 *Proc. IEEE Nuclear Science Symposium Conference,* November 9–15, 1997, Albuquerque, NM, USA, p. 1697

[17] Yan Y and Zeng G L 2009 *Int. J. Imaging Sys. Technol.* **19** 271

[18] Chantler C T, Olsen K, Dragoset R A, Chang J, Kishore A R, Kotochigova S A and Zucker D S 1995 *J. Phys. Chem. Ref. Data* **24** 71

[19] Ben Bouallegue F, Crouzet J F, Comtat C, Fourcade M, Mohammadi B and Mariano-Goulart D 2007 *IEEE Trans. Med. Imaging* **26** 1001

[20] Hudson H M and Larkin R S 1994 *IEEE Trans. Med. Imaging* **13** 601